

# Impact of Van der Waals interactions on structural and nonlinear optical properties of azobenzene switches

Carmelo Naim,<sup>†,‡</sup> Frédéric Castet,<sup>\*,‡</sup> and Eduard Matito<sup>\*,†,¶</sup>

<sup>†</sup>*Donostia International Physics Center (DIPC), Manuel Lardizabal Ibilbidea 4, 20018*

*Donostia, Euskadi, Spain*

<sup>‡</sup>*Institut des Sciences Moléculaires (ISM, UMR CNRS 5255), University of Bordeaux, 351*

*Cours de la Libération, 33405 Talence, France*

<sup>¶</sup>*Ikerbasque Foundation for Science, Plaza Euskadi 5, 48009 Bilbao, Euskadi, Spain*

E-mail: frederic.castet@u-bordeaux.fr; ematito@gmail.com

## Abstract

The geometrical structures, relative *Z-E* energies, and second-order nonlinear responses of a collection of azobenzene molecules symmetrically substituted in *meta*-position with functional groups of different bulkiness are investigated using various *ab initio* and DFT levels of approximation. We show that RI-MP2 and RI-CC2 approximations provide very similar geometries and relative energies and evidence that London dispersion interactions existing between bulky *meta*-substituents stabilize the *Z* conformer. The  $\omega$ B97-X-D exchange-correlation functional provides an accurate description of these effects and gives a good account of the nonlinear optical response of the molecules. We show that density functional approximations should include no less than 50% of Hartree-Fock exchange to provide accurate hyperpolarizabilities. A property-structure analysis of the azobenzene derivatives reveals that the main contribution to

the first hyperpolarizability comes from the azo bond, but phenyl *meso*-substituents can enhance it.

## Introduction

Materials and molecules that exhibit large second-order nonlinear optical properties (NLOs), *i.e.*, whose dielectric polarization responds quadratically to the electric-field component of light, find applications in laser components, optical communications, data processing, and storage<sup>1,2</sup> as well as in bioimaging and therapy.<sup>3-5</sup> In addition to the quest for materials able to deliver high second harmonic generation (SHG) responses, an important research topic in the field is the design of new molecular systems with commutable second-order NLOs. Indeed, such systems that can isomerize between two (or more) stable and reversibly interconvertible forms with a large difference in their first hyperpolarizabilities ( $\beta$ ) present high interest for exploitation in optoelectronic and photonic devices, such as high-density optical memories with multiple storages and nondestructive readout capacity.<sup>6-8</sup>

Since light is a fast, non-invasive, and low-cost way to trigger the interconversion between the different isomeric forms, photochromic molecules constitute the most prominent class of candidates for eventual exploitation in NLO devices. One of the most studied families of photochromes that exhibit large  $\beta$  contrasts is that of double-bond isomer derivatives, which undergo a reversible isomerization between a stable *trans* (E) and a metastable *cis* (Z) form upon illumination in the UV range. Among them, azobenzene derivatives have been the subject of many theoretical and experimental investigations, mostly due to the high first hyperpolarizabilities obtained when adding donor and acceptor groups to both ends of the azobenzene core.<sup>9-16</sup> Reversible SHG switching in solid-state structures incorporating azobenzenes as NLO functional units was also demonstrated, whether in poled polymers,<sup>17,18</sup> LB films,<sup>7</sup> liquid-crystalline polymers,<sup>19,20</sup> or self-assembled monolayers.<sup>21-24</sup> Recent theoretical works also highlighted that azobenzene NLO switches could be exploited as versatile

probes for phase recognition in biological environments.<sup>25,26</sup>

At the molecular level, it is well known that the nature of the chemical substituents determines the relative thermodynamic stability of the *trans* and *cis* forms of azobenzene derivatives and thus plays a critical role in their photo-isomerization process. In particular, chemical functionalization in the *meta*-position with bulky substituents has been shown to lower the *cis*  $\rightarrow$  *trans* thermal reaction rates due to the attractive London dispersion forces that stabilize the *cis* isomer.<sup>27</sup> In addition to their key role in the structure and photochemical processes of molecular switches, Van der Waals interactions are also expected to impact their NLO properties. However, although the impact of London dispersion forces on molecular properties has recently received some attention,<sup>28–30</sup> their influence on the NLOs of molecular switches has been overlooked thus far.

In this work, we report a comprehensive theoretical study of the structural and NLO properties of a collection of azobenzene molecules symmetrically substituted in *meta*-position with functional groups of different bulkiness (Figure 1). In the first part, we address the performance of a large set of density functional approximations (DFAs) for calculating the geometries and relative energies of the E and Z isomers by using the second-order approximate coupled-cluster singles and doubles (CC2) results as the theoretical reference. Computational results are also compared to previously reported data.<sup>27</sup> In the second part, we investigate the accuracy of the different DFAs for reproducing the static first hyperpolarizability of the *cis* forms compared to *ab initio* second-order Møller–Plesset (MP2) and CC2 calculations. Finally, we use the partition of NLOs in terms of orbital contributions (PNOC)<sup>31</sup> to decipher the individual role of the *meta*-substituents on the NLO responses of this series of compounds.

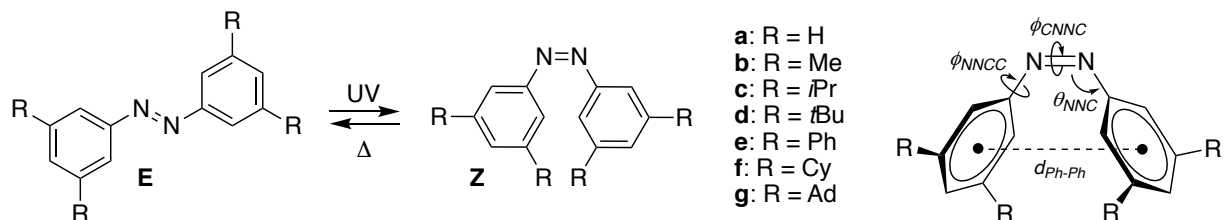


Figure 1: Substituted azobenzene derivatives investigated in this study (Cy = cyclohexyl, Ad = adamantyl) and geometrical parameters used to characterize the *cis* conformers.

## Computational methodology

Reference geometries were optimized at the CC2 level<sup>32</sup> using the Resolution of Identity (RI)<sup>33</sup> and frozen core approximations. In Table S1, based on the results of the Diet-GMTKN55 benchmark set,<sup>34</sup> we show that CC2 and MP2 offer very similar performance for intramolecular noncovalent interactions (MAE below 2 kcal/mol and RMSE below 1.5 kcal/mol for both methods). The cc-pVDZ basis set<sup>35</sup> was used in all calculations and employed as the auxiliary basis for RI computations.<sup>36</sup> This basis set guarantees a good compromise between accuracy and computational cost because it provides very similar geometrical structures and energy differences between *Z* and *E* isomers as those obtained using the more extended cc-pVTZ basis set (see Tables S2 and S3). The energy convergence threshold in both single-point SCF and CC calculations has been set to  $10^{-6}$  a.u. RI-MP2, a wide range of DFAs (see Table S4), and the Hartree-Fock (HF) method were tested to address their ability to reproduce reference RI-CC2 structures. HF completely neglects electron correlation and thus is expected to perform poorly in the systems affected by dispersion. It is included here as a means to quantify the amount of electron correlation (and dispersion) introduced by the other methods. The selected DFAs involve two different dispersion correction schemes: the Grimme’s D3 scheme<sup>37–40</sup> and the nonlocal Van Der Waals density functional (VV) scheme developed by Vydrov and Van Voorhis.<sup>41</sup> To size up the impact of these corrections on the molecular structures, calculations were also performed using the uncorrected counterparts of the DFAs.

In order to confirm the single-reference nature of the title molecules, we have performed the D1 diagnostics<sup>42</sup> on the CC2 wavefunctions. In all cases, D1 values are close to the threshold value of 0.05, indicating the partial multireference character of these wavefunctions (see Table S5). We have also computed the  $I_{ND}$  index<sup>43,44</sup> obtained from the range-separation partition of the Coulomb hole.<sup>45,46</sup>  $I_{ND}$  is proportional to the deviation from idempotency of the first-order reduced density matrix.<sup>47,48</sup> In all cases,  $I_{ND}$  values are rather small compared to other multireference molecules<sup>49</sup> (see Table S5). All in all, we can conclude that these molecules present a rather mild multireference character and they can be reasonably well described with single-reference methods such as MP2 and CC2.

The selected set of DFAs was then employed to evaluate the static components of the first hyperpolarizability tensor (*i.e.*, in the zero frequency limit) of the azobenzene derivatives, as well as the total first hyperpolarizability defined as follows:

$$\beta(0; 0, 0) = \beta = \frac{1}{5} \sqrt{\beta_x^2 + \beta_y^2 + \beta_z^2} \quad (1)$$

where

$$\beta_i = \sum_{j=x,y,z} (\beta_{ijj} + \beta_{jij} + \beta_{jji}) \quad (2)$$

and  $i=x,y,z$ . Since *trans* forms have a centrosymmetric shape with no second-order NLO responses,  $\beta$  values were calculated for *cis* forms only. Reference values were computed using a finite field (FF) differentiation procedure of the CC2 and MP2 electronic energies. For the compound with the adamantyl substituent, NLOP calculations were performed only at the CAM-B3LYP level due to computational limitations. A Romberg scheme<sup>50,51</sup> was employed to control and improve the accuracy of the numerical derivatives, employing field amplitudes starting from  $\pm 0.001$  a.u. with a multiplicative step of 1.4142. All first hyperpolarizability calculations were performed using the aug-cc-pVTZ basis set. The pertinent integrals resulting from the electronic energy calculation using DFAs were done numerically using the "Ultrafine" integration grid involving 99 radial shells around each atom and 590 angular

points per shell. RI-CC2 and RI-MP2 calculations were performed with TURBOMOLE,<sup>52</sup> where the RIJK approximation was employed in addition to the RI approximation for some of the largest molecules (**d**-Z, **e**-Z, and **f**-Z) since it has been shown to reduce the computational cost without affecting the accuracy of the energies.<sup>53</sup> Calculations using DFAs involving the VV approximation were performed with Qchem,<sup>54</sup> whereas calculations involving all other DFAs were performed with Gaussian 16.<sup>55</sup> The root mean square deviation (RMSD) of distances between equivalent atoms of the two molecules has been calculated to quantify the structural differences of two optimized geometries. The RMSD of two structures was calculated using the software provided in Ref. 56. This program calculates the RMSD between two Cartesian geometries using the Kabsch algorithm (1976)<sup>57</sup> or Quaternion algorithm<sup>58</sup> if rotation is needed before calculating RMSD. Following the authors recommendation, we have excluded the hydrogen atoms in the calculation of the RMSD. For the sake of completeness, the RMSD values including all the atoms in the molecules are given in Tables S10-11.

## Results and discussion

### Structure and relative energies of the conformers

#### Reference *ab initio* calculations

Table 1 reports selected structural parameters of the *cis* isomers calculated at the HF, RI-MP2, and RI-CC2 levels with the cc-pVDZ basis set, namely, the N=N and C-N bond lengths ( $d_{NN}$  and  $d_{CN}$ ), the N=N-C bond angles ( $\theta_{NNC}$ ), the torsional angles around the N=N and C-N bonds ( $\phi_{CNNC}$  and  $\phi_{NNCC}$ ), as well as the distance  $d_{PhPh}$  between the centroids of the two phenyl rings (see Figure 1). As expected, geometries calculated using HF, which does not account for dispersion effects, significantly differ from the MP2 and CC2 ones. In particular, HF N=N distances are shorter, while the  $\theta_{NNC}$  and  $\phi_{NNCC}$  angles are larger, resulting in larger  $d_{PhPh}$  distances between the lateral phenyl rings.

The geometries calculated using MP2 and CC2 are quite similar (largest RMSD=0.08 Å, see Table S8),  $d_{NN}$ ,  $d_{CN}$ ,  $\theta_{NNC}$ , and  $\phi_{CNNC}$  barely changing from one compound to another. In contrast,  $d_{PhPh}$  and  $\phi_{NNCC}$ , which are directly linked to the relative orientation of the *meta*-substituents, show slight variations. These two geometrical parameters reflect the interplay between attractive dispersion interactions and repulsive steric hindrance. For MP2 and CC2, the  $d_{PhPh}$  distance mostly decreases when increasing the size of the R groups as a consequence of the increase of the dispersion interactions. However, the size of the substituents is not the only factor controlling the strength of the noncovalent interaction. Compound **e** (R = Ph) exhibits the smallest  $d_{NN}$  value within the series, owing to the planar shape of the phenyl substituents that allows larger spatial overlap and hence larger attractive London dispersion forces, together with the possibility to adopt a relative spatial orientation minimizing the steric hindrance (**e** also has the smallest  $\phi_{NNCC}$  and the largest  $\phi_{CNNC}$ ). Taken as a whole, the geometrical parameters of the *cis* conformer computed at the CC2 and MP2 levels clearly evidence the balance between repulsive steric hindrance and attractive VdW interactions: increasing the bulkiness of the substituents in *meta* position both enhances steric repulsion and dispersion attraction, resulting in slight changes in the geometry of the central part of the compounds. The enhancement of attractive non-covalent interactions (NCI) as the bulkiness of *meta*-substituents increases is further illustrated in Figure 2, where the surface area of the NCI isosurface clearly increases with the size of R. In Table S6, we collect the geometrical data of the *trans* conformers, which are far less affected by electron correlation. Indeed, only  $d_{NN}$  is stretched upon the inclusion of electron correlation, the differences between CC2 and MP2 being insignificant.

As demonstrated recently,<sup>27</sup> the existence of these attractive VdW interactions has a crucial impact on the thermodynamics of the isomerization reaction by stabilizing the *cis* form relative to the *trans* one. As shown in Figure 3 and Table S12, HF calculations do not reproduce these effects correctly and provide very similar energy differences between the two

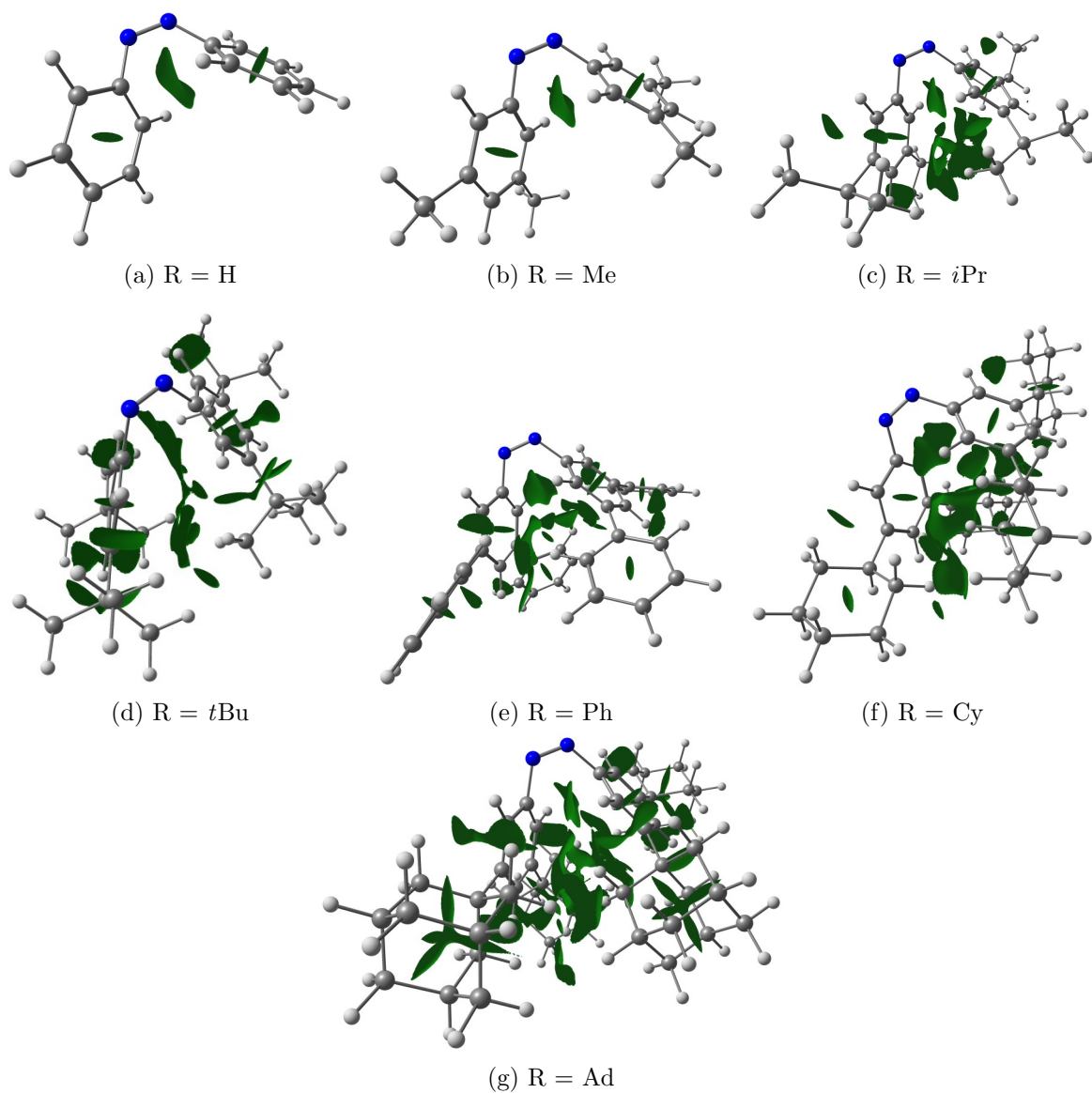


Figure 2: Isosurfaces indicating the regions of weakly attractive intramolecular noncovalent interactions (NCI) in the different molecules, generated using the NCI software<sup>59,60</sup> with the promolecular density obtained from the CC2 geometries.



Table 1: Characteristic distances and angles of the *cis* isomers of compounds **a-g** (see Figure 1), as calculated at the RI-CC2/cc-pVDZ level (see also Table S6 for *trans* isomers).

Molecule	$d_{NN}$ [Å]	$d_{NC}$ [Å]	$d_{PhPh}$ [Å]	$\theta_{NNC}$ [°]	$\phi_{CNNC}$ [°]	$\phi_{NNCC}$ [°]
HF/cc-pVDZ						
<b>a</b> (R = H)	1.215	1.43	4.60	123.9	-5.0	-58.2
<b>b</b> (R = Me)	1.215	1.44	4.59	123.8	-4.9	-60.3
<b>c</b> (R = <i>i</i> Pr)	1.215	1.44	4.58	123.8	-5.0	-60.0
<b>d</b> (R = <i>t</i> Bu)	1.215	1.44	4.60	124.0	-5.2	-59.7
<b>e</b> (R = Ph)	1.215	1.44	4.58	123.6	-4.7	-58.9
<b>f</b> (R = Cy)	1.215	1.44	4.58	123.8	-5.0	-59.8
<b>g</b> (R = Ad)	1.215	1.44	4.60	124.0	-5.2	-59.0
RI-MP2/cc-pVDZ						
<b>a</b> (R = H)	1.271	1.44	4.42	120.7	-6.8	-53.9
<b>b</b> (R = Me)	1.272	1.44	4.43	121.0	-6.6	-52.5
<b>c</b> (R = <i>i</i> Pr)	1.275	1.44	4.15	119.1	-6.2	-56.9
<b>d</b> (R = <i>t</i> Bu)	1.276	1.44	4.12	119.1	-6.8	-55.1
<b>e</b> (R = Ph)	1.277	1.45	3.91	117.8	-4.7	-60.2
<b>f</b> (R = Cy)	1.276	1.44	4.14	119.0	-6.7	-56.9
<b>g</b> (R = Ad)	1.277	1.44	4.05	118.6	-6.9	-55.8
RI-CC2/cc-pVDZ						
<b>a</b> (R = H)	1.269	1.43	4.40	121.0	-7.6	-52.7
<b>b</b> (R = Me)	1.279	1.45	4.40	120.9	-5.9	-51.1
<b>c</b> (R = <i>i</i> Pr)	1.282	1.45	4.16	119.1	-6.5	-56.2
<b>d</b> (R = <i>t</i> Bu)	1.283	1.45	4.12	119.0	-6.8	-55.0
<b>e</b> (R = Ph)	1.284	1.45	3.92	117.8	-5.3	-59.6
<b>f</b> (R = Cy)	1.282	1.45	4.14	119.0	-7.0	-56.4
<b>g</b> (R = Ad)	1.284	1.45	4.07	118.9	-5.7	-54.1

isomers ( $\Delta E_{EZ}$ ) for all compounds, as a result of the neglect of dispersion interactions. On the contrary, both CC2 and MP2 calculations confirm the lowering of  $\Delta E_{EZ}$  when increasing the bulkiness of the R groups. Although CC2 provides slightly smaller  $\Delta E_{EZ}$  values than MP2, we note the good agreement between these two levels of approximation, with differences in the  $\Delta E_{EZ}$  values smaller than 1.0 kcal/mol for compounds **a-e** and equal to 1.25 kcal/mol for **f**. A larger deviation (1.87 kcal/mol) is obtained for the largest compound **g** (R = Ad).

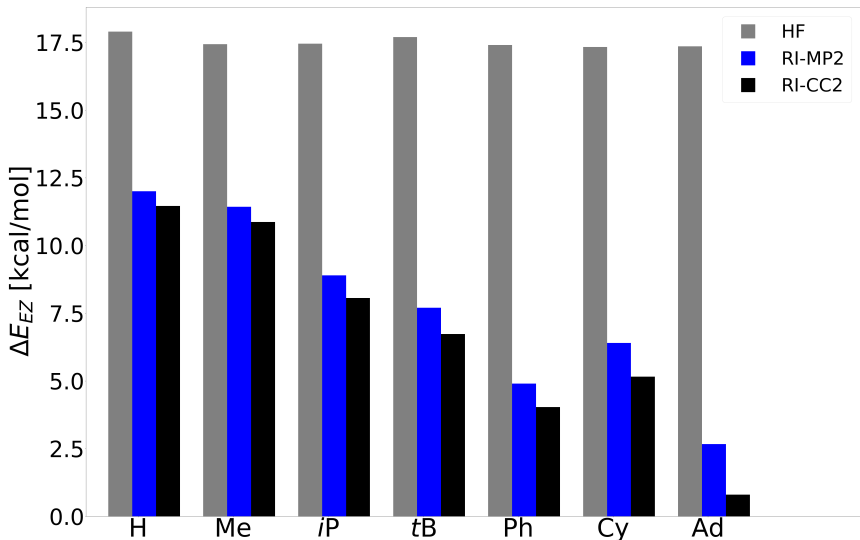


Figure 3: Difference in the energy of the *trans* (E) and *cis* (Z) forms,  $\Delta E_{EZ} = E_Z - E_E$ , as calculated at the HF, RI-MP2, and RI-CC2 levels with the cc-pVDZ basis set.

### DFT calculations

Using the CC2 results as a reference, we now analyze the performance of different DFAs in reproducing the geometrical structures and relative energies of the *trans* and *cis* forms of the investigated series of azobenzenes. As above, the similarity between DFT and CC2 geometries is measured for both the *trans* and *cis* isomers forms using the RMSD of atomic positions.

In the Supporting Information, we report the differences in the geometries provided by the DFAs including D3 or VV dispersion corrections and their uncorrected counterparts. As expected, the RMSD values reported in Table S7 and Figures S1 and S2 show that structural differences are small for *trans* isomers and large for *cis* isomers (in particular for compounds incorporating bulky substituents). The RMSD values calculated for *cis* isomers using  $\omega$ B97X-D and, especially, M06-2X-D3 are much smaller than those calculated using the other selected DFAs, which confirms that these functionals already include some dispersion corrections in their native form.<sup>61,62</sup>

Geometries of the *cis* isomers optimized using dispersion-corrected DFAs are compared to CC2 geometries in Figure 4. The results clearly show that adding dispersion corrections using either the D3 or VV scheme largely improves the matching with the reference geometries. Although acceptable results are obtained with all the tested dispersion-corrected functionals,  $\omega$ B97-X-D shows the smallest average RMSD (0.10 Å), followed by M06-2X-D3 (0.13 Å), LC- $\omega$ PBE08-VV (0.14 Å), B3LYP-D3 (0.16 Å), PBE0-D3 and CAM-B3LYP-D3 (both at 0.17 Å). The values of all the RMSD averaged over the total number of compounds are collected in Table S9.

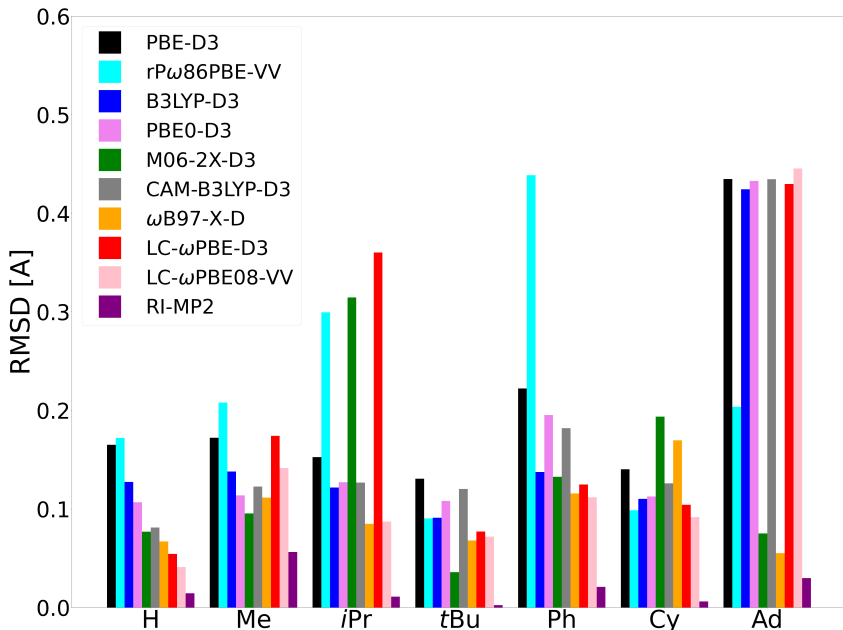


Figure 4: RMSD excluding hydrogen atoms between DFAs and CC2 geometries for *cis* isomers. RI-MP2 results are also shown for comparison.

We now analyze the performance of the selected DFAs in reproducing the energy difference between the two isomers optimized at the corresponding level of theory (Figure 5 and Table S13). The best agreement with CC2  $\Delta E_{ZE}$  values is obtained with the LC- $\omega$ PBE-D3 and  $\omega$ B97-X-D functionals, which display average errors of 1.40 and 1.57 kcal/mol, respectively, for the molecular series. Interestingly, among the studied DFAs,  $\omega$ B97-X-D was

already the best functional to obtain accurate geometries. On the other hand, notice that the molecule with  $R = \text{Ph}$  gives rise to errors of at least 3 kcal/mol for all the functionals considered. As we can check in Table S14, it is not due to a wrong estimation of the geometry with these DFAs. Finally, for the sake of completeness, we also calculated the differences in the Gibbs free energies (Table S13). In general,  $\Delta G_{ZE}$  follows the same trend as  $\Delta E_{ZE}$ , showing a strong reduction upon addition of dispersion corrections to compounds bearing bulky *meta*-substituents.

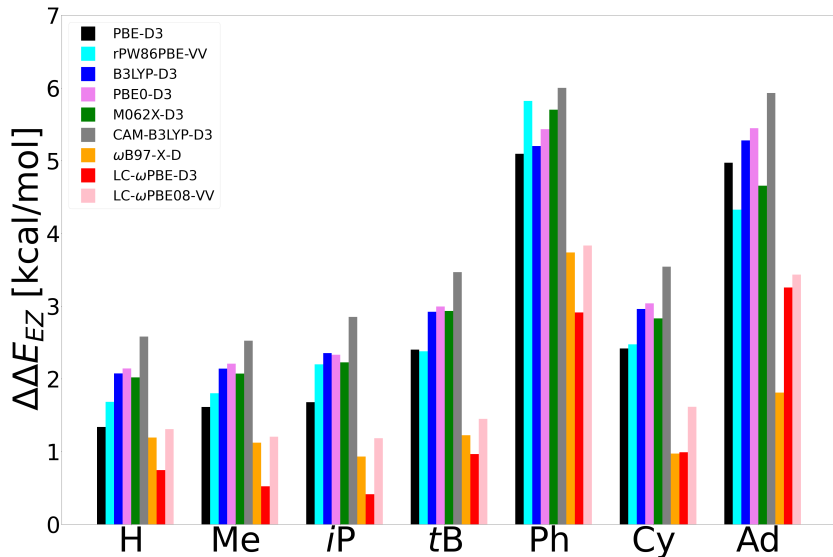


Figure 5: Differences in the *Z-E* isomerization energies calculated at the CC2 level and at the DFT level using DFAs with dispersion corrections ( $\Delta\Delta E_{ZE} = \Delta E_{ZE}(DFT) - \Delta E_{ZE}(CC2)$ , in kcal/mol).

## Second-order NLO properties

### Reference *ab initio* calculations

Hereafter, all the calculations will be performed using the geometries optimized at RI-CC2/cc-pVDZ level of theory. The total static first hyperpolarizabilities (Eq. 1) of the *cis* isomers, calculated at the HF, MP2, and CC2 *ab initio* levels are reported in Table 2.

Comparison of MP2 and CC2  $\beta$  values with HF ones provides a direct assessment of the magnitude of electron correlation effects. The first hyperpolarizability increases from HF to MP2, as expected from the localized nature of HF densities. Going from MP2 to CC2 further increases the  $\beta$  values. An excellent linear correlation is obtained between MP2 and CC2  $\beta$  values (see Figure 6), with a very small intercept, suggesting that MP2 values are systematically 64% smaller than CC2 ones. Hence, the trends among different compounds are perfectly reproduced using either MP2 or CC2, and it thus indifferent which method we employ for benchmarking. We will choose MP2 values as the reference ones because their absolute values provide a better agreement with most DFAs (*vide infra*). Notice also that despite the complete neglect of electron correlation, for the first five molecules of the series, HF static polarizabilities also show a very good linear correlation with the MP2 counterparts (see Figure 6). Compound **e** (R = Ph) is not shown in the latter figure and it will be discussed in detail in the following section.

Table 2: Total static first hyperpolarizabilities ( $\beta$ , a.u.) calculated using different *ab initio* levels of approximation together with the aug-cc-pVTZ basis set.

Molecule	HF	MP2	CC2
<b>a</b> (R = H)	7.7	52.5	80.8
<b>b</b> (R = Me)	40.7	119.3	161.7
<b>c</b> (R = <i>i</i> Pr)	31.6	99.8	148.5
<b>d</b> (R = <i>t</i> Bu)	32.9	84.1	136.1
<b>e</b> (R = Ph)	21.3	152.4	239.8
<b>f</b> (R = Cy)	50.7	127.7	191.0
<b>g</b> (R = Ad)	60.2	-	-

## DFT calculations

We now address the performance of DFAs in reproducing the static first hyperpolarizability of the azobenzene derivatives **a-f**. Since D3 corrections do not affect the electronic density, D3-corrected functionals are excluded from the benchmark. DFAs incorporating dispersion effects through the VV scheme are considered. The latter will be informative about the

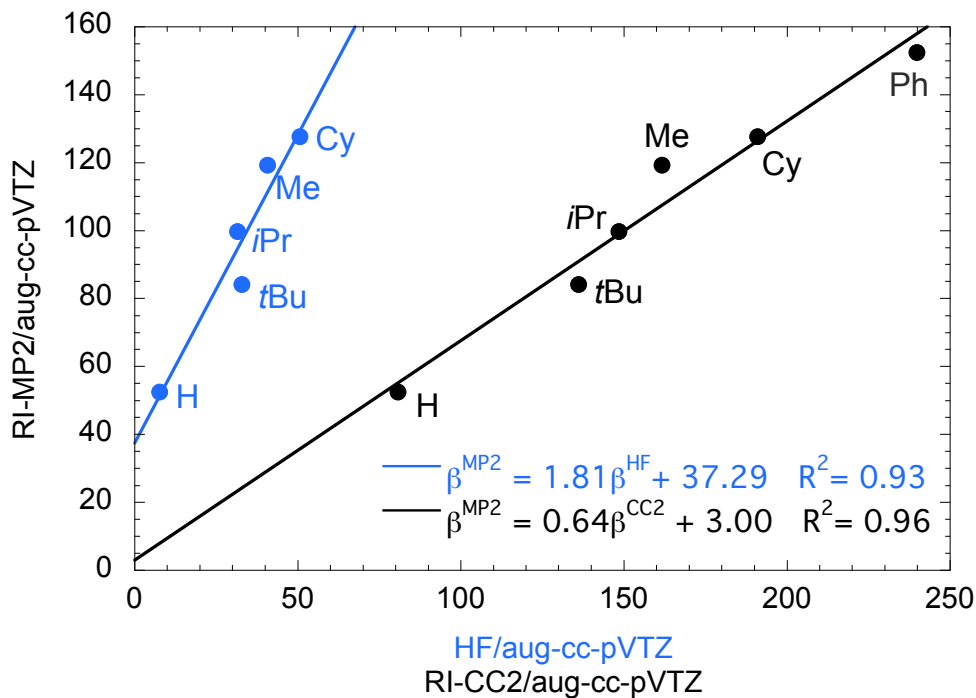


Figure 6: Correlation between static hyperpolarizabilities ( $\beta$ , a.u.) of the series of azobenzenes calculated at the MP2 level with respect to the values calculated using CC2 and HF. The  $\beta$  value calculated for compound **e** ( $R = \text{Ph}$ ) is excluded from the fit in HF calculations.

effect of dispersion corrections in the calculation of nonlinear optical properties, beyond the indirect effect of dispersion on the geometries.

In the last three columns of Table 3, we collect three different measures of the error committed in the hyperpolarizability using a collection of DFAs and RI-CC2 with respect to RI-MP2. These data are reported in Figure 6 for all molecules except **g** ( $R = \text{Ad}$ ). The three DFAs that provide the lowest mean absolute error (MAE), mean absolute percentage error (MAPE), and root mean square deviation (RMSD) are CAM-B3LYP, M06-2X, and  $\omega\text{B97X-D}$  (unlike other dispersion-corrected DFAs,  $\omega\text{B97X-D}$  employs a different parameterization than the native functional,  $\omega\text{B97X}$ ). Hence, the latter functionals, which outperform RI-CC2, provide the closest agreement to the RI-MP2 hyperpolarizability values. However, these results would hide the fact that if we are only concerned about the relative magnitude of hyperpolarizability among the compounds, many other methods work just fine. The latter is even more relevant if we consider the difficulty in reproducing absolute values of

nonlinear optical properties and the fact that we are using RI-MP2 values for comparison, which are approximate too. Table 3 provides the results for the linear regression of RI-MP2 vs. other methods using all the molecules except for compounds **e** ( $R = \text{Ph}$ ) and **g** ( $R = \text{Ad}$ ); we will use the former compound’s results to measure the ability of the methods to provide a correct trend of the hyperpolarizability for this series of compounds. The Pearson coefficient,  $R^2$ , shows that 9 out of 20 methods (including RI-CC2, CAM-B3LYP, and M06-2X) give excellent results ( $R^2 \geq 0.95$ ) for the five smallest compounds of the series. The difference between the value predicted by the linear regression and the MP2 hyperpolarizability,  $\Delta\beta^{Ph} = \hat{\beta}^{Ph,\text{meth}} - \beta^{Ph,\text{MP2}}$ , provides an estimate of the predictability of the linear regression for molecule **e** including phenyl *meso*-substituents. Despite the excellent correlations found for the first five compounds, only six methods give an estimate of  $\beta^{Ph,\text{MP2}}$  with an error below 20 a.u. (RI-CC2, PBE, rPW86-PBE-VV, M06, M06L, and M06-2X). It is worth noticing that the data for M06L does not include the results calculated for compound **c** ( $R = \text{iPr}$ ), because it was not possible to obtain numerically stable energy calculations with an external field. For many DFAs and RI-CC2, the value of the intercept ( $b$ ) is rather small (below 20 a.u.) and the Pearson coefficient is rather high. In these cases, the prediction of  $\beta$  is dominated by the slope,  $a$ , which determines whether the quantity is overestimated ( $a < 1$ ) or underestimated ( $a > 1$ ) with respect to the RI-MP2 values. Our conjecture is that, in the latter DFAs, the error on the hyperpolarizability is dominated by the delocalization error. In Figure 7, we represent the % of HF exchange at long range (large  $r_{12}$ ) that is included in the XCF against the value of  $a$ . The plot reflects clearly how DFAs with a small percentage of HF exchange tend to overestimate the hyperpolarizability with respect to RI-MP2, whereas the opposite occurs for DFAs with a large percentage of HF exchange (see also Tables S16-S17). If we consider all the measures included in Table 3, the best performing DFA is M06-2X. We also obtain quite good results using CAM-B3LYP,  $\omega\text{B97-X-D}$ , and  $\text{T}\alpha\text{-LC-BLYP}$ . All these functionals include at least 54% of HF exchange at long range. Hence, a percentage of nearly 50% between DFT and HF exchange is the adequate balance for computing the

NLO properties of these systems, as it was also concluded from previous works on smaller molecules<sup>63</sup> and conjugated push-pull chromophores.<sup>64,65</sup> These results thus contribute to the recent findings about the importance of the delocalization error in the calculation of linear and nonlinear optical properties.<sup>64,66–69</sup> It is worth noticing that the recent strategy<sup>69</sup> of finding the optimal range-separation parameter to calculate  $\gamma$  from the values of  $\alpha$  works quite well to calculate the value of  $\beta$  for these systems. Indeed, T $\alpha$ -LC-BLYP and LC-BLYP give a similar Pearson coefficient, whereas for the former  $a$  and  $b$  are closer to 1 and 0, respectively. As a result, T $\alpha$ -LC-BLYP significantly improves MAE, MAPE, and RMSD.

Table 3: Results of the linear correlation between the MP2 hyperpolarizabilities and several other methods, together with several error measures (see text). The linear regression function is:  $\hat{\beta}^{\text{MP2}} = a\beta^{\text{meth}} + b$ , where  $\beta^{\text{meth}}$  is value of the hyperpolarizability for one the methods listed in the table.  $\Delta\beta^{\text{Ph}} = \hat{\beta}^{\text{Ph,meth}} - \beta^{\text{Ph,MP2}}$ . For M06L, compound **c** (R = iPr) was excluded from the analysis because its results suffer from large numerical instabilities.

Method	a	b [a.u.]	$\Delta\hat{\beta}^{\text{Ph}}$ [a.u.]	R <sup>2</sup>	RMSD [a.u.]	MAPE [%]	MAE [a.u.]
RI-CC2	0.72	-6.98	-13.72	0.96	56.75	34	53.68
HF	1.81	37.29	76.48	0.93	80.18	318	75.15
PBE	0.52	4.57	10.23	0.84	90.69	45	86.87
rPW86-PBE	0.28	38.85	41.73	0.68	119.55	49	107.03
rPW86-PBE-VV	0.52	-0.87	-0.77	0.88	102.73	48	98.33
PBE0	0.91	-14.05	22.00	0.97	23.18	18	21.55
B3LYP	0.85	-18.98	22.37	0.96	37.21	27	36.14
BH&H	1.22	4.26	25.71	0.96	29.44	32	26.27
CAM-B3LYP	1.11	-7.42	49.61	0.96	22.22	13	13.24
$\omega$ B97-X	1.12	3.78	54.46	0.91	31.32	27	22.52
$\omega$ B97X-D	0.97	-5.19	53.57	0.88	21.62	16	16.19
LC-BLYP	1.32	20.43	60.79	0.93	54.40	94	48.89
T $\alpha$ -LC-BLYP	1.11	0.72	57.32	0.94	29.75	24	20.02
LC- $\omega$ PBE	1.26	10.86	57.70	0.95	44.17	59	37.93
LC- $\omega$ PBE08	1.33	15.59	56.13	0.95	50.45	79	45.18
LC- $\omega$ PBE08-VV	1.30	17.54	48.07	0.95	48.37	75	43.99
M06	0.73	-16.27	17.24	0.86	59.20	36	57.85
M06L	0.60	-31.31	16.32	0.88	95.74	37	76.88
M06-2X	1.15	-0.06	19.53	0.97	19.45	18	16.36
M06-HF	1.27	47.23	59.12	0.86	71.55	693	67.37

Regarding the impact of dispersion corrections,  $\beta$  values computed using rPW86PBE-VV show an improvement compared to those computed with its uncorrected parent. Although



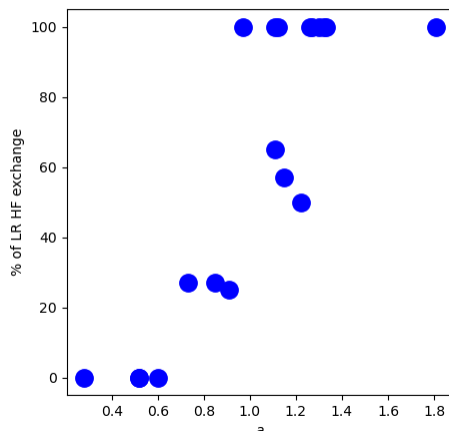


Figure 7: Results of the fit of the  $a$  parameter correlated with the % of Long Range HF exchange for each functional included in the set.

some error measurements like RSMD, MAE, or MAPE are only marginally improved upon including of VV dispersion corrections,  $\Delta\beta^{Ph}$ ,  $a$  and the Pearson coefficient are much better for rPW86PBE-VV. Conversely, LC- $\omega$ PBE08-VV and LC- $\omega$ PBE08 show a similar performance. Finally, going from  $\omega$ B97X to  $\omega$ B97X-D significantly improves the RSMD, MAE, and MAPE, while only slightly modifies the linear regression plot; *i.e.*, both functionals give similar trends among the series of compounds but  $\omega$ B97X-D provide better estimates of the MP2 hyperpolarizabilities. It is worth stressing that the differences in the  $\beta$  values computed using the two latter functionals cannot be only ascribed to dispersion corrections since the whole set of their parameters (including the range separation,  $\omega$ ) is different.

### Partition of the hyperpolarizability into orbital contributions

To gain a deeper insight into the contribution of the *meta*-substituents to the total first hyperpolarizability, we now examine in more detail the vector ( $\beta_i$ ) and tensor ( $\beta_{ijk}$ ) components of the total first hyperpolarizability (Eqs. 1 and 2) of the investigated compounds. A common Cartesian frame, in which the origin is placed at the center of the N=N bond, the  $x$  axis is oriented along this bond, and the  $xz$  plane contains the two nitrogen atoms and one of the adjacent carbon atom (see Figure 8) is used for all the molecules. CAM-

B3LYP/aug-cc-pVTZ hyperpolarizabilities are considered in the analyses since, as discussed in the previous section, they are in close agreement with the absolute MP2 reference values. As shown in Table 4, the  $\beta_z$  component is one order of magnitude larger than  $\beta_x$  and  $\beta_y$  in all compounds, except for compound **g** (R = Ad) for which  $\beta_z/\beta_y = 3.55$ , the larger contribution from the  $y$  being due to bulkiness of the adamantyl substituent. In turn, decomposition of  $\beta_z$  in terms of tensor elements evidence that the dominant contribution to the first hyperpolarizability arises from the transverse  $\beta_{zxx}$  component. Note that, as shown in SI (Table S19), a very similar picture of the relative magnitude of the  $\beta$  components can be drawn from CAM-B3LYP calculations carried out using the smaller 6-311++G\*\* basis set.

Table 4: Vector ( $\beta_i$ ) and tensor ( $\beta_{ijk}$ ) components of the total first hyperpolarizability, as calculated at the CAM-B3LYP/aug-cc-pVTZ level. The Cartesian frame used for the calculations is shown in Figure 8.

Molecule	$\beta$	$\beta_x$	$\beta_y$	$\beta_z$	$\beta_{zxx}$	$\beta_{zyy}$	$\beta_{zzz}$
<b>a</b> (R = H)	52	0	-17	-261	-135	21	27
<b>b</b> (R = Me)	115	0	-30	-576	-159	-14	-19
<b>c</b> (R = <i>i</i> Pr)	93	-4	-7	-463	-149	16	-22
<b>d</b> (R = <i>t</i> Bu)	91	-82	50	-447	-167	43	-25
<b>e</b> (R = Ph)	100	-1	22	-498	-122	-62	19
<b>f</b> (R = Cy)	119	60	28	-592	-144	-33	-20
<b>g</b> (R = Ad)	148	-9	-201	-714	-170	2	-69

To rationalize the role of molecular substituents in the value of the hyperpolarizability, we use the PNO scheme developed by Sitkiewicz and coworkers<sup>31</sup> to decompose the NLO responses into contributions of the molecular orbitals (MOs) of the unperturbed system:

$$\beta_{ijk} = \sum_p \beta_{ijk,p} = - \sum_p \Delta_{pp}^{(jk)} M_{pp}^{(i)} - \sum_{p \neq q} \Delta_{pq}^{(jk)} M_{pq}^{(i)}, \quad (3)$$

where  $\mathbf{M}^i$  is the transition dipole matrix along the  $i$  direction, and  $\Delta^{(jk)}$  is the second-order derivative of the one-particle reduced density matrix with respect to external fields oriented along  $j$  and  $k$  axes. This expression is an exact decomposition of  $\beta$  based on the assumption

that the terms that depend on two different MOs can be equally distributed between them. In this framework, for an orthonormal set of orbitals, a real-space representation of the largest  $\beta_{zxx}$  component can be obtained according to:

$$\beta_{zxx}(\vec{r}) = \sum_p \beta_{zxx,p} |\phi_p(\vec{r})|^2, \quad (4)$$

where  $|\phi_p(\vec{r})|^2$  is the square of the amplitude of molecular orbital  $p$ . The PNOC representations of  $\beta_{zxx}(\vec{r})$  in the Cartesian space are displayed in Figure 8 for the azobenzene series at the CAM-B3LYP/6-311++G\*\* level. The main contribution to the first hyperpolarizability arises from the N=N bond for all the molecules, although for bulkier substituents there are also important contributions. Some contributions are due to *ortho* and *para* carbon atoms of the adjacent phenyl rings, although, in general, the adjacent phenyl ring shows rather small contributions to  $\beta$ . Interestingly, the phenyl substituents in compound **e** (R = Ph) show an important contribution to  $\beta$  from  $\pi$  orbitals. In compounds **c**, **d**, **f**, and **g**,  $\beta_{zxx}(\vec{r})$  also show contributions due to C-C  $\sigma$ -bonds of the R alkyl groups, although larger contributions from the substituents are obtained for bulkier substituents such as cyclohexyl and adamantyl.

Individual orbital contribution analysis reveals that the hyperpolarizability of these compounds cannot be qualitatively explained from the contribution of a few molecular orbitals. Many MOs must be included in the summation of the Eq. 3 to obtain a good estimate of the total  $\beta_{zxx}$  component (see Figure S12), hampering a simple deconvolution of the total NLO response in terms of individual MOs. However, for all compounds except **e** (R = Ph), the highest occupied MO, which is mainly associated with the  $p$  orbitals of the nitrogen atoms (the  $\pi$  orbitals and the lone pairs) and to the C-N  $\sigma$  bonds, provides the largest contribution to  $\beta_{zxx}$  (Table S20).

Finally, we have used the PNOC as a tool to analyze the delocalization errors committed by some DFAs. As a measure of the extent of electron delocalization, we have computed the Laplacian of the electron density,<sup>70</sup>  $\nabla^2 \rho(\vec{r})$ , which attains large negative values in delocalized

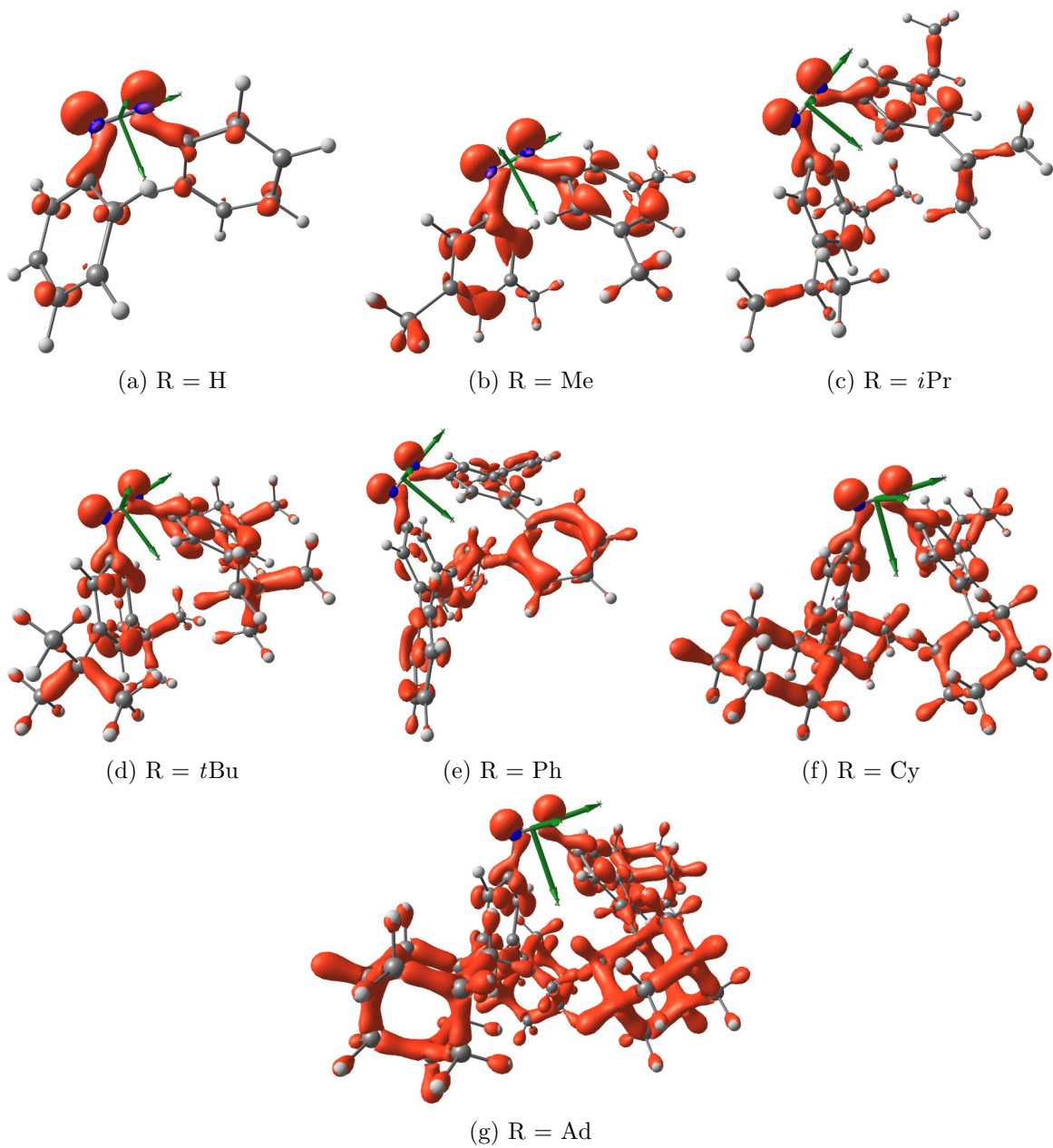


Figure 8: Isosurfaces of  $\beta_{zxx}(\vec{r})$  for the azobenzene molecules obtained using the PNOCC partition at the CAM-B3LYP/6-311++G\*\* level. Isocontour values of  $\pm 5$  a.u. were used for all compounds.

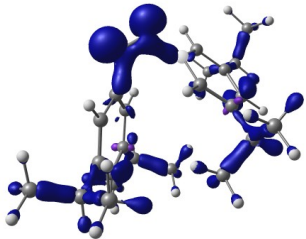
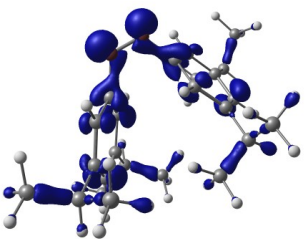
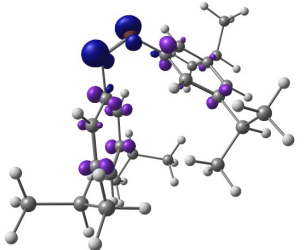
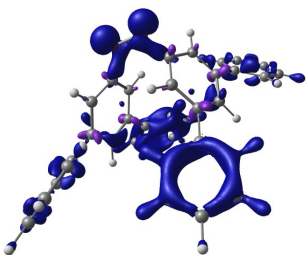
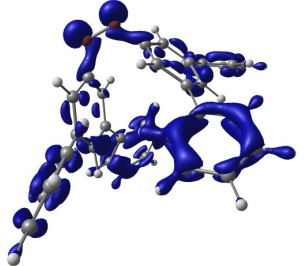
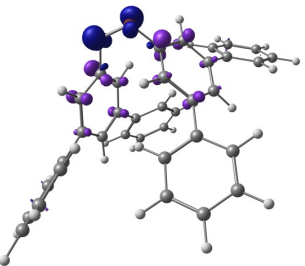
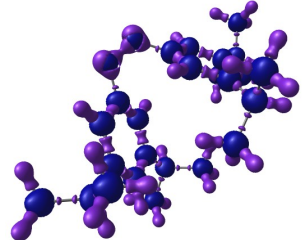
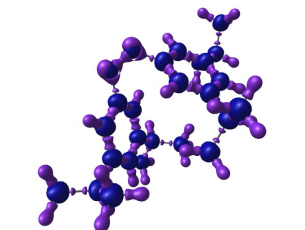
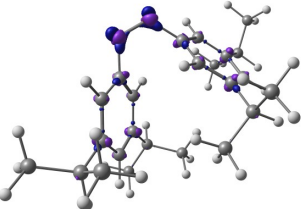
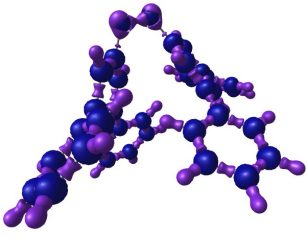
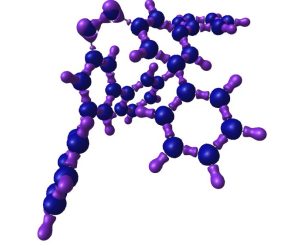
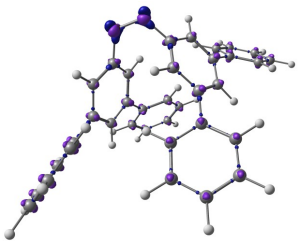
regions. Table 5 gives PNOC and  $\nabla^2\rho(\vec{r})$  values for **e** (R = Ph) and **c** (R = *i*Pr) at the PBE and CAM-B3LYP levels of theory. Since PBE suffers from larger delocalization errors than CAM-B3LYP, it is expected that both the PNOC and  $-\nabla^2\rho(\vec{r})$  display regions with larger values for PBE. In order to clearly visualize these differences, in Table 5, we have also plotted the difference between these two DFAs. For both molecules, the main difference in the distribution of the hyperpolarizability across the molecule comes from the lone pair of the nitrogen atoms.  $\Delta\nabla^2\rho(\vec{r})$  values are also larger around the nitrogen atoms. Hence, one is deemed to conclude that the delocalization error is the main source of error in the calculation of the hyperpolarizability and it comes mostly from a wrong description of the electron density in the vicinity of the N=N bond (in particular, the *p* orbitals involved in the  $\pi$  bond and the lone pairs).

## Conclusions

The reliability of a large selection of exchange-correlation density functional approximations to predict the geometrical structure, relative Z-E energies ( $\Delta E_{ZE}$ ), and second-order nonlinear responses of a series of azobenzene molecules has been assessed with respect to reference correlated *ab initio* calculations carried out at the RI-MP2 and RI-CC2 levels. Our calculations show that RI-MP2 and RI-CC2 approximations provide very similar performance for intramolecular noncovalent interactions, based on the results of Diet-GMTKN55 and the series of azobenzene molecules studied in this paper. Comparisons with Hartree-Fock results show that electron correlation and, in particular, dispersion interactions are the driving forces behind the stabilization of the *cis* conformer with respect to the *trans* one. Indeed, the *cis* isomer stabilizes upon functionalization of the *meta*-position with bulky substituents that develop mutual attractive London interactions.

Among the selected dispersion-corrected exchange-correlation functionals,  $\omega$ B97-X-D provides the closest agreement with reference RI-CC2 geometries and  $\Delta E_{ZE}$  values. CAM-

Table 5: Comparison of  $\beta_{zxx}(\vec{r})$  calculated through PNOC for the functionals PBE and CAM-B3LYP evaluated for the molecules **c** (R = *i*Pr) and **e** (R = Ph). The isosurface  $\Delta\beta_{zxx}(\vec{r})$  is calculated as:  $\Delta\beta_{zxx}(\vec{r}) = \beta_{zxx}^{(PBE)} - \beta_{zxx}^{(CAM-B3LYP)}$ . Isocontour values of  $\pm 5$  a.u. were used for all the  $\beta_{zxx}$ . For the Laplacian of the electronic density isocontour  $\pm 0.7$  was used for the Laplacians, while  $\pm 0.09$  was used for the difference between the laplacian ( $\Delta\nabla^2$ ) of the PBE and the CAM-B3LYP densities. Positive numbers are displayed in blue, negative ones in purple.

Molecule	$\beta_{zxx}(\vec{r})^{(PBE)}$	$\beta_{zxx}(\vec{r})^{(CAM-B3LYP)}$	$\Delta\beta_{zxx}(\vec{r})$
R = <i>i</i> Pr			
R = Ph			
Molecule	$\nabla^2\rho(\vec{r})^{(PBE)}$	$\nabla^2\rho(\vec{r})^{(CAM-B3LYP)}$	$\Delta\nabla^2\rho(\vec{r})$
R = Ph			
R = Ph			

B3LYP-D3 and LC- $\omega$ PBE-D3 also provide reasonably good geometries, the latter giving excellent  $\Delta E_{ZE}$  values too.

This study shows an excellent linear correlation between static first hyperpolarizabilities computed at the RI-MP2 and RI-CC2 levels using RI-CC2 geometries. RI-MP2 provides  $\beta$  values systematically underestimated compared to RI-CC2. Despite density functional approximations do not give accurate first hyperpolarizabilities, many of the selected functionals qualitatively reproduce the evolution of  $\beta$  along the series of azobenzene derivatives. The most accurate functionals are CAM-B3LYP,  $\omega$ B97-X-D, and T $\alpha$ -LC-BLYP. In general, the best performing functionals include at least 50% of the exact HF exchange.  $\omega$ B97X-D seems to be the best suited functional to describe all the relevant features of these compounds: the geometry, the energy difference between the isomers, and the first hyperpolarizabilities.

Subsequently, we analyzed the property-structure relationship for the first hyperpolarizability of azobenzene derivatives to identify the effect of the *meta*-substituents on the NLO responses. For all molecules, the dominant contribution to  $\beta$  comes from the  $\beta_{zxx}$  tensor component. The PNOC decomposition analysis<sup>31</sup> was employed to analyze the molecular orbitals and the real-space contributions to the optical response. A simple inspection of the orbital contributions shows that it is impossible to obtain a simple description of the total first hyperpolarizability in terms of few orbital contributions. However, the PNOC real-space analysis reveals that the main contribution to  $\beta$  comes mostly from N=N, followed by smaller contributions from the adjacent phenyl rings. Interestingly, phenyl substituents attached in *meso* of the adjacent phenyl rings also show important contributions from the  $\pi$  system to the first hyperpolarizability.

Finally, we studied the relationship between the real-space PNOC analysis and the delocalization error. We found a qualitative correlation between the electron delocalization differences (measured through the Laplacian of the electron density) and the real-space PNOC representations. Hence, it seems that the regions of the molecule most affected by the delocalization error are, in turn, the ones responsible for the inaccuracy of the first

hyperpolarizability.

## Acknowledgement

The authors thank Josep M. Luis and Sebastian P. Sitkiewicz for helpful discussions. C.N. acknowledges the University of Bordeaux Initiative of Excellence (IDEX) for his Ph.D. grant. This work was supported by the French National Research Agency (grant number ANR-20-CE29-0009-01) and by the Transnational Common Laboratory QuantumChemPhys (Theoretical Chemistry and Physics at the Quantum Scale, grant number ANR-10-IDEX-03-02) established between the Université de Bordeaux (UB), Euskal Herriko Unibertsitatea (UPV/EHU) and Donostia International Physics Center (DIPC). This research was also funded by Spanish MINECO (grant numbers PGC2018-098212-B-C21 and EUR2019-103825) and the Basque Government / Eusko Jaurlaritza (GV/EJ) (grant numbers IT1254-19, PIBA19-0004, and 2019-CIEN-000092-01). Calculations were performed on the computing facilities provided by the DIPC and the Mésocentre de Calcul Intensif Aquitain (MCIA) of the University of Bordeaux and of the Université de Pau et des Pays de l'Adour. Technical and human support provided by IZO-SGI, SGIker (UPV/EHU, MICINN, GV/EJ, ERDF, and ESF), and MCIA is gratefully acknowledged.

## Supporting Information Available

The Supporting Information contains...

## References

- (1) Dalton, L. R.; Sullivan, P. A.; Bale, D. H. Electric Field Poled Organic Electro-optic Materials: State of the Art and Future Prospects. *Chem. Rev.* **2010**, *110*, 25–55.



- (2) Stegeman, G. I.; Stegeman, R. A. In *Nonlinear Optics: Phenomena, Materials and Devices*; Boreman, G., Ed.; John Wiley and Sons: Hoboken, NJ, 2012.
- (3) Campagnola, P. J.; Wei, M. D.; Loew, L. M. High-Resolution Nonlinear Optical Imaging of Live Cells by Second Harmonic Generation. *Biophys. J.* **1999**, *77*, 3341–3349.
- (4) Moreaux, L.; Sandre, O.; Charpak, S.; Blanchard-Desce, M.; Mertz, J. Coherent Scattering in Multi-Harmonic Light Microscopy. *Biophys. J.* **2001**, *80*, 1568–1574.
- (5) Reeve, J. E.; Anderson, H. L.; Clays, K. Dyes for biological second harmonic generation imaging. *Phys. Chem. Chem. Phys.* **2010**, *12*, 13484–13498.
- (6) Coe, B. J. Molecular Materials Possessing Switchable Quadratic Nonlinear Optical Properties. *Chem. Eur. J.* **1999**, *5*, 2464–2471.
- (7) Delaire, J. A.; Nakatani, K. Linear and Nonlinear Optical Properties of Photochromic Molecules and Materials. *Chem. Rev.* **2000**, *100*, 1817–1846.
- (8) Castet, F.; Rodriguez, V.; Pozzo, J.-L.; Ducasse, L.; Plaquet, A.; Champagne, B. Design and Characterization of Molecular Nonlinear Optical Switches. *Acc. Chem. Res.* **2013**, *46*, 2656–2665.
- (9) Ledoux, I.; Zyss, J.; Barni, E.; Barolo, C.; Diulgheroff, N.; Quagliotto, P.; Viscardi, G. Properties of novel azodyes containing powerful acceptor groups and thiophene moiety. *Synthetic Metals* **2000**, *115*, 213 – 217.
- (10) Yesodha, S. K.; Sadashiva Pillai, C. K.; Tsutsumi, N. Stable polymeric materials for nonlinear optics: a review based on azobenzene systems. *Progress in Polymer Science* **2004**, *29*, 45 – 74.
- (11) Krawczyk, P.; Kaczmarek, A.; Zaleśny, R.; Matczyszyn, K.; Bartkowiak, W.; Ziółkowski, M.; Cysewski, P. Linear and nonlinear optical properties of azobenzene derivatives. *Journal of Molecular Modeling* **2009**, *15*, 581–590.

- (12) Pérez-Moreno, J.; Zhao, Y.; Clays, K.; Kuzyk, M. G.; Shen, Y.; Qiu, L.; Hao, J.; Guo, K. Modulated Conjugation as a Means of Improving the Intrinsic Hyperpolarizability. *Journal of the American Chemical Society* **2009**, *131*, 5084–5093.
- (13) Kleinpeter, E.; Bölke, U.; Kreicberga, J. Quantification of the push-pull character of azo dyes and a basis for their evaluation as potential nonlinear optical materials. *Tetrahedron* **2010**, *66*, 4503–4509.
- (14) Cardoso, C.; Abreu, P. E.; Milne, B. F.; Nogueira, F. Computational Study of Molecules with High Intrinsic Hyperpolarizabilities. *The Journal of Physical Chemistry A* **2010**, *114*, 10676–10683.
- (15) Jaunet-Lahary, T.; Chantzis, A.; Chen, K. J.; Laurent, A. D.; Jacquemin, D. Designing Efficient Azobenzene and Azothiophene Nonlinear Optical Photochromes. *The Journal of Physical Chemistry C* **2014**, *118*, 28831–28841.
- (16) Ghanavatkar, C. W.; Mishra, V. R.; Sekar, N. Review of NLOphoric azo dyes—Developments in hyperpolarizabilities in last two decades. *Dyes and Pigments* **2021**, *191*, 109367.
- (17) Loucif-Saibi, R.; Nakatani, K.; Delaire, J. A.; Dumont, M.; Sekkat, Z. Photoisomerization and second harmonic generation in disperse red one-doped and -functionalized poly(methyl methacrylate) films. *Chem. Mater.* **1993**, *5*, 229–236.
- (18) Sekkat, Z.; Prêtre, P.; Knoesen, A.; Volksen, W.; Lee, V. Y.; Miller, R. D.; Wood, J.; Knoll, W. Correlation between polymer architecture and sub-glass-transition-temperature light-induced molecular movement in azo-polyimide polymers: influence on linear and second- and third-order nonlinear optical processes. *J. Opt. Soc. Am. B* **1998**, *15*, 401–413.
- (19) Vijay Srinivasan, M.; Kannan, P. Photo-switching and nonlinear optical behaviors of

- center linked bent-core azobenzene liquid crystalline polymers. *Journal of Materials Science* **2011**, *46*, 5029–5043.
- (20) Priimagi, A.; Ogawa, K.; Virkki, M.; Mamiya, J.-i.; Kauranen, M.; Shishido, A. High-Contrast Photoswitching of Nonlinear Optical Response in Crosslinked Ferroelectric Liquid-Crystalline Polymers. *Advanced Materials* **2012**, *24*, 6410–6415.
- (21) Yamada, K.; Otsubo, H.; Yonemura, H.; Yamada, S.; Matsuo, T. Nonlinear Optical Responses of Dialkoxiazobenzene Isomers Adsorbed to Interface between Heptane and Viologen-Modified Quartz Plates. *Chemistry Letters* **1997**, *26*, 451–452.
- (22) Schulze, M.; Utecht, M.; Moldt, T.; Przyrembel, D.; Gahl, C.; Weinelt, M.; Saalfrank, P.; Tegeder, P. Nonlinear optical response of photochromic azobenzene-functionalized self-assembled monolayers. *Phys. Chem. Chem. Phys.* **2015**, *17*, 18079–18086.
- (23) Tonnelé, C.; Champagne, B.; Muccioli, L.; Castet, F. Nonlinear Optical Contrast in Azobenzene-Based Self-Assembled Monolayers. *Chemistry of Materials* **2019**, *31*, 6759–6769.
- (24) Riaz, S.; Friedrichs, G. Vibrational sum-frequency generation study of molecular structure, sterical constraints and nonlinear optical switching contrast of mixed alkyl-azobenzene self-assembled monolayers. *Zeitschrift für Physikalische Chemie* **2020**, *234*, 1427 – 1452.
- (25) Osella, S.; Knippenberg, S. Triggering On/Off States of Photoswitchable Probes in Biological Environments. *Journal of the American Chemical Society* **2017**, *139*, 4418–4428.
- (26) Knippenberg, S.; Osella, S. Push/Pull Effect as Driving Force for Different Optical Responses of Azobenzene in a Biological Environment. *The Journal of Physical Chemistry C* **2020**, *124*, 8310–8322.

- (27) Schweighauser, L.; Strauss, M. A.; Bellotto, S.; Wegner, H. A. Attraction or Repulsion? London Dispersion Forces Control Azobenzene Switches. *Angewandte Chemie International Edition* **2015**, *54*, 13436–13439.
- (28) Aradhya, S. V.; Frei, M.; Hybertsen, M. S.; Venkataraman, L. Van der Waals interactions at metal/organic interfaces at the single-molecule level. *Nature Materials* **2012**, *11*, 872–876.
- (29) Wagner, J. P.; Schreiner, P. R. London Dispersion in Molecular Chemistry—Reconsidering Steric Effects. *Angewandte Chemie International Edition* **2015**, *54*, 12274–12296.
- (30) Fabrizio, A.; Corminboeuf, C. How do London Dispersion Interactions Impact the Photochemical Processes of Molecular Switches? *The Journal of Physical Chemistry Letters* **2018**, *9*, 464–470.
- (31) Sitkiewicz, S. P.; Rodríguez-Mayorga, M.; Luis, J. M.; Matito, E. Partition of optical properties into orbital contributions. *Phys. Chem. Chem. Phys.* **2019**, *21*, 15380–15391.
- (32) Christiansen, O.; Koch, H.; Jørgensen, P. The second-order approximate coupled cluster singles and doubles model CC2. *Chem. Phys. Lett.* **1995**, *243*, 409–418.
- (33) Hättig, C.; Weigend, F. CC2 excitation energy calculations on large molecules using the resolution of the identity approximation. *J. Chem. Phys.* **2000**, *113*, 5154–5161.
- (34) Gould, T. ‘Diet GMTKN55’ offers accelerated benchmarking through a representative subset approach. *Phys. Chem. Chem. Phys.* **2018**, *20*, 27735–27739.
- (35) Dunning Jr., T. H. Gaussian basis sets for use in correlated molecular calculations. I. The atoms boron through neon and hydrogen. *J. Chem. Phys.* **1989**, *90*, 1007–1023.
- (36) Hättig, C. Optimization of auxiliary basis sets for RI-MP2 and RI-CC2 calculations:

- Core-valence and quintuple- $\zeta$  basis sets for H to Ar and QZVPP basis sets for Li to Kr. *Phys. Chem. Chem. Phys.* **2005**, *7*, 59–66.
- (37) Grimme, S. Semiempirical GGA-type density functional constructed with a long-range dispersion correction. *Journal of Computational Chemistry* **2006**, *27*, 1787–1799.
- (38) Grimme, S.; Antony, J.; Ehrlich, S.; Krieg, H. A consistent and accurate ab initio parametrization of density functional dispersion correction (DFT-D) for the 94 elements H-Pu. *The Journal of Chemical Physics* **2010**, *132*, 154104.
- (39) Grimme, S.; Ehrlich, S.; Goerigk, L. Effect of the damping function in dispersion corrected density functional theory. *Journal of Computational Chemistry* **2011**, *32*, 1456–1465.
- (40) Grimme, S. Density functional theory with London dispersion corrections. *WIREs Computational Molecular Science* **2011**, *1*, 211–228.
- (41) Vydrov, O. A.; Van Voorhis, T. Nonlocal van der Waals density functional: The simpler the better. *The Journal of Chemical Physics* **2010**, *133*, 244103.
- (42) Lee, T. J. Comparison of the T1 and D1 diagnostics for electronic structure theory: a new definition for the open-shell D1 diagnostic. *Chem. Phys. Lett.* **2003**, *372*, 362–367.
- (43) Ramos-Cordoba, E.; Salvador, P.; Matito, E. Separation of dynamic and nondynamic correlation. *Phys. Chem. Chem. Phys.* **2016**, *18*, 24015–24023.
- (44) Ramos-Cordoba, E.; Matito, E. Local Descriptors of dynamic and nondynamic correlation. *J. Chem. Theory Comput.* **2017**, *13*, 2705–2711.
- (45) Via-Nadal, M.; Rodríguez-Mayorga, M.; Ramos-Cordoba, E.; Matito, E. Singling out Weak and Strong Correlation. *J. Phys. Chem. Lett.* **2019**, *10*.
- (46) Via-Nadal, M.; Rodríguez-Mayorga, M.; Ramos-Cordoba, E.; Matito, E. Range Separation of the Coulomb Hole. **submitted**,

- (47) Löwdin, P.-O. Quantum theory of many-particle systems. I. Physical interpretations by means of density matrices, natural spin-orbitals, and convergence problems in the method of configurational interaction. *Phys. Rev.* **1955**, *97*, 1474–1489.
- (48) Smith Jr, V. H. Approximate natural orbitals for carbon 1 S. *Theor. Chim. Acta (Berlin)* **1967**, *7*, 245.
- (49) Sitkiewicz, S.; Ramos-Cordoba, E.; Luis, J. M.; Matito, E. How Many Electrons Does a Molecular Electride Hold? *J. Phys. Chem. A* doi:10.1021/acs.jpca.1c02760, accepted.
- (50) de Wergifosse, M.; Liégeois, V.; Champagne, B. Evaluation of the molecular static and dynamic first hyperpolarizabilities. *Int. J. Quant. Chem.* **2014**, *114*, 900–910.
- (51) Champagne, B.; Beaujean, P.; de Wergifosse, M.; Cardenuto, M. H.; Liégeois, V.; Castet, F. In *Frontiers of Quantum Chemistry*; Wojcik, M., Nakatsuji, H., Kirtman, B., Ozaki, Y., Eds.; Springer, Singapore, 2018; Chapter Quantum Chemical Methods for Predicting and Interpreting Second-Order Nonlinear Optical Properties: From Small to Extended  $\pi$ -Conjugated Molecules, pp 117–138.
- (52) Balasubramani, S. G. et al. TURBOMOLE: Modular program suite for ab initio quantum-chemical and condensed-matter simulations. *The Journal of Chemical Physics* **2020**, *152*, 184107.
- (53) Weigend, F. A fully direct RI-HF algorithm: Implementation, optimised auxiliary basis sets, demonstration of accuracy and efficiency. *Phys. Chem. Chem. Phys.* **2002**, *4*, 4285–4291.
- (54) Shao, Y. et al. Advances in molecular quantum chemistry contained in the Q-Chem 4 program package. *Mol. Phys.* **2015**, *113*, 184–215.
- (55) Frisch, M. J. et al. Gaussian~16 Revision C.01. 2016; Gaussian Inc. Wallingford CT.

- (56) Charnley, J.; Bratholm, L. Calculate Root-mean-square deviation (RMSD) of Two Molecules Using Rotation. GitHub, v.1.3.2.
- (57) Kabsch, W. A solution for the best rotation to relate two sets of vectors. *Acta Crystallographica Section A: Crystal Physics, Diffraction, Theoretical and General Crystallography* **1976**, *32*, 922–923.
- (58) Walker, M. W.; Shao, L.; Volz, R. A. Estimating 3-D location parameters using dual number quaternions. *CVGIP: image understanding* **1991**, *54*, 358–367.
- (59) Johnson, E. R.; Keinan, S.; Mori-Sánchez, P.; Contreras-García, J.; Cohen, A. J.; Yang, W. Revealing noncovalent interactions. *J. Am. Chem. Soc.* **2010**, *132*, 6498–6506.
- (60) Contreras-García, J.; Johnson, E. R.; Keinan, S.; Chaudret, R.; Piquemal, J.-P.; Beratan, D. N.; Yang, W. NCIPLOT: a program for plotting noncovalent interaction regions. *J. Chem. Theory Comput.* **2011**, *7*, 625–632.
- (61) Zhao, Y.; Truhlar, D. G. The M06 Suite of Density Functionals for Main Group Thermochemistry, Thermochemical Kinetics, Noncovalent Interactions, Excited States, and Transition Elements: two New Functionals and Systematic Testing of Four M06-Class Functionals and 12 Other Functionals. *Theor. Chem. Acc.* **2008**, *120*, 215–241.
- (62) Chai, J.-D.; Head-Gordon, M. Systematic optimization of long-range corrected hybrid density functionals. *The Journal of Chemical Physics* **2008**, *128*, 084106.
- (63) Castet, F.; Champagne, B. Assessment of DFT Exchange-Correlation Functionals for Evaluating the Multipolar Contributions to the Quadratic Nonlinear Optical Responses of Small Reference Molecules. *Journal of Chemical Theory and Computation* **2012**, *8*, 2044–2052.

- (64) Johnson, L. E.; Dalton, L. R.; Robinson, B. H. Optimizing Calculations of Electronic Excitations and Relative Hyperpolarizabilities of Electrooptic Chromophores. *Acc. Chem. Res.* **2014**, *47*, 3258–3265.
- (65) Lescos, L.; Sitkiewicz, S.; Beaujean, P.; Blanchard-Desce, M.; Champagne, B. R.; Matito, E.; Castet, F. Performance of DFT Functionals for Calculating the Second-Order Nonlinear Optical Properties of Dipolar Merocyanines. *Phys. Chem. Chem. Phys.* **2020**, 16579–16594.
- (66) Champagne, B.; Perpète, E. A.; Jacquemin, D.; van Gisbergen, S. J. A.; Baerends, E.-J.; Soubra-Ghaoui, C.; Robins, K. A.; Kirtman, B. Assessment of Conventional Density Functional Schemes for Computing the Dipole Moment and (Hyper)polarizabilities of Push–Pull  $\pi$ -Conjugated Systems. *J. Phys. Chem. A* **2000**, *104*, 4755–4763.
- (67) de Wergifosse, M.; Champagne, B. Electron correlation effects on the first hyperpolarizability of push–pull  $\pi$ -conjugated systems. *J. Chem. Phys.* **2011**, *134*, 074113.
- (68) Zalesny, R.; Medved', M.; Sitkiewicz, S. P.; Matito, E.; Luis, J. M. Can Density Functional Theory Be Trusted for High-Order Electric Properties? The Case of Hydrogen-Bonded Complexes. *J. Chem. Theory Comput.* **2019**, *15*, 3570–3579.
- (69) Besalú-Sala, P.; Sitkiewicz, S. P.; Salvador, P.; Matito, E.; Luis, J. M. A new tuned range-separated density functional for the accurate calculation of second hyperpolarizabilities. *Phys. Chem. Chem. Phys.* **2020**, *22*, 11871–11880.
- (70) Bader, R. F. W. *Atoms in Molecules: A Quantum Theory*; Oxford University Press: Oxford, 1990.